

StainedView: Variable-Intensity Light-Attenuation Display with Cascaded Spatial Color Filtering for Improved Color Fidelity

Takumi Kaminokado, Yuichi Hiroi, and Yuta Itoh

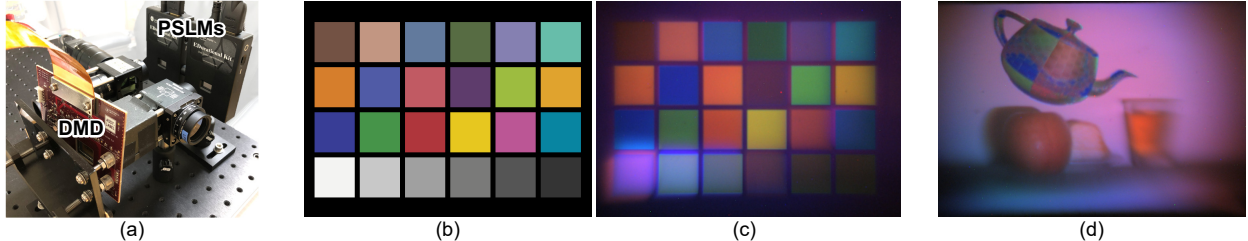


Fig. 1. (a) Proof-of-concept system. Primary components (two PSLMs and the DMD) are annotated. (b) An example of a target image (Macbeth chart). (c) Observed image. (d) Another example in an AR context. A virtual teapot is rendered over a real table.

Abstract—We present StainedView, an optical see-through display that spatially filters the spectral distribution of light to form an image with improved color fidelity. Existing light-attenuation displays have limited color fidelity and contrast, resulting in a degraded appearance of virtual images. To use these displays to present virtual images that are more consistent with the real world, we require three things: intensity modulation of incoming light, spatial color filtering with narrower bandwidth, and appropriate light modulation for incoming light with an arbitrary spectral distribution. In StainedView, we address the three requirements by cascading two phase-only spatial light modulators (PSLMs), a digital micromirror device, and polarization optics to control both light intensity and spectrum distribution. We show that our design has a 1.8 times wider color gamut fidelity (75.8% fulfillment of sRGB color space) compared to the existing single-PSLM approach (41.4%) under a reference white light. We demonstrated the design with a proof-of-concept display system. We further introduce our optics design and pixel-selection algorithm for the given light input, evaluate the spatial color filter, and discuss the limitation of the current prototype.

Index Terms—Light attenuation display, phase modulation, see-through display, vision augmentation, augmented reality.

1 INTRODUCTION

Optical see-through head-mounted displays (OST-HMDs) play an essential role in a variety of existing augmented reality (AR) applications, including entertainment, communications, healthcare, and manufacturing, by overlaying virtual objects on the user’s field of view (FoV) [24].

All OST-HMDs follow the principal optical design of the prototype developed by Ivan Sutherland [41]. The optical design augments computer-generated images into the user’s field of view in an *additive* manner. A beam splitter, typically a prism or a waveguide in modern designs, guides the light coming from an internal display into the user’s eye, thus working as an optical beam combiner. Because beam splitters also path light from the real world, existing OST-HMDs inherit the color blending problem, in which the user perceives a semitransparent, low contrast image degraded by the background light from the real scene [11, 27].

A variety of methods have been proposed to solve this color blending problem, including an optical method to attenuate the background light by attaching a visor that dims the entire OST-HMD, which is common in commercial OST-HMDs [4], and a software method to adjust the display color according to the background color by capturing the scene with a first-person camera [27]. A more fundamental solution is to

add an optical occlusion layer to the OST-HMD [23, 43]. By using a transmissive LCD or a reflective liquid crystal on silicon (LCoS), the optical occlusion layer blocks the external light spatially passing through the OST-HMD by switching the opacity of each pixel.

Even if optical occlusion is used to avoid the color blending problem, additive displays are still affected by ambient light. In particular, in outdoor use, it is necessary to increase the brightness of the display in response to the brightness of ambient light, which leads to an increase in power consumption. Because of the size and weight limitations of the wearable display, the battery capacity is also limited, so the brightness value cannot be increased indefinitely (even if the brightness limits that the small built-in display can emit are ignored). For this reason, it is difficult to use OST-HMDs outdoors.

As long as designs rely on the additive optics inherited from Sutherland’s display design, these brightness problems will persist. As a distinct yet complementary paradigm, displays based on light subtraction address these problems. In the subtractive display paradigm, a display creates an image from the background light by displaying a spatial color filter. Because the subtractive display is merely a passive spatial color filter, it does not need internal power to display a bright image as if observing the sunlight through stained glass. Essentially, the maximum light intensity of subtractive displays is proportional to the brightness of the outside scene. The problem of insufficient brightness to the environment, which is a problem with additive OST-HMDs, cannot in principle arise in subtractive displays.

As a proof-of-concept system of subtractive displays, Itoh et al. proposed light-attenuation display (LAD) [17]. Their system combines a phase-only spatial light modulator (PSLM) with polarization optics to extend the monochromatic light occlusion approach to color-stylized subtraction from the incident light. Their system can display different spatial color filters for each pixel by controlling the phase-shift value of each pixel on the PSLM. Their reflective design can also achieve

• *Takumi Kaminokado is with Tokyo Institute of Technology, E-mail: kaminokado@arc.titech.ac.jp.*
• *Yuichi Hiroi is with Tokyo Institute of Technology, E-mail: yuichi.hiroi@arc.titech.ac.jp.*
• *Yuta Itoh is with Tokyo Institute of Technology, E-mail: yuta.itoh@arc.titech.ac.jp.*

This work has been submitted to the IEEE for possible publication. Copyright may be transferred without notice, after which this version may no longer be accessible. Upon acceptance of the article by IEEE, the preprint article must be replaced with the accepted version, as described in the section Accepted article.

higher resolution compared to those using color LCDs [47], because each pixel can represent colors instead of using RGB Bayer patterns.

Although LAD has correctly demonstrated the advantages of subtractive displays, it has two fundamental drawbacks in terms of image quality. The first is the inability to uniformly modulate the transmission intensity, and the second is the color fidelity—that is, the bandwidth of the color filter is too wide. The former means that LAD can express hue but not brightness, and the latter means that its color gamut is small. Considering that existing additive OST-HMDs have as good color reproducibility as regular monitors, the image quality problem in LAD must be resolved.

In this study, we thus address these issues by proposing StainedView, a subtractive OST-HMD that realizes high contrast and wide-color-range images (Fig. 1). We cascade a digital micromirror device (DMD) with two PSLMs and control the PSLMs based on an end-to-end theoretical analysis of its polarization optics. Adding the DMD as an amplitude modulator allows us to control the intensity. Cascading two PSLMs theoretically gives extra room to expand the color gamut of the displayed color filter. In their previous study of LAD [17], as a preliminary pilot experiment for future work, they investigated cascading PSLMs to improve the color gamut by measuring some colors through a simple two-PSLMs setup. However, they did not provide a working system that meets the following technical requirements:

1. Spatial alignment of PSLM layers to modulate each light ray in the field of view
2. Realization of the desired color filter by controlling the phase modulation of multiple PSLMs based on theoretical polarization interference analysis
3. Algorithm with which to compute the DMD and phase images based on a desired color filter image

Note that using a DMD is one of the options for amplitude modulation. Other possible implementations will be discussed in Sec. 8.

Overall, this paper contributes to the subtractive display knowledge by providing an end-to-end theoretical analysis of the color filter via multiple PSLMs and an amplitude modulator. It also provides practical knowledge on implementing a system while building a proof-of-concept prototype. Our analysis is far more advanced than the previous LAD study in terms of taking into account the spectral performance of all optical components in use, resulting in optimized color simulation.

Our main contributions are as follows:

- Presenting an intensity-modulated subtractive OST display with a color range of 75.8% sRGB fulfillment wider than the existing single-PSLM approach (of 41.4%)
- Providing an end-to-end theoretical foundation for realizing the system with polarization optics under a see-through optical design
- Sharing calibration processes to properly refine the performance of the cascaded optical system
- Demonstrating our proof-of-concept monocular system in both simulation and measurement under an AR setup

2 RELATED WORK

2.1 Head-Mounted Displays with Spatial Light Occlusion

The subtractive display is based on the same optical design concept as occlusion-capable OST-HMDs. Occlusion-capable OST-HMDs use spatial light modulators (SLMs) capable of modulating the amplitude (intensity). For example, a transmissive LCD can control the opacity of each pixel; thus, it functions as an optical occlusion mask [21–23, 52]. Another example is reflective LCoS displays, which can control the reflectance of incident light in each pixel [5, 12, 13, 48]. DMDs switch the direction of reflection of incident light on a pixel-by-pixel basis; thus, they can function as optical occlusion masks if the optical system is designed such that one reflection direction is assigned to the scene and the other to a light-absorbing material [20, 26, 46].

As described above, using SLMs can realize optical occlusion. However, to achieve functioning occlusion-capable OST-HMDs, an optical focusing system needs to be integrated. A simple approach is the relay optical system [22]. The system binds an SLM with two lenses of a focal length of f with the distance $2f$. Then, background at infinite distance is focused on the spatial modulator. Finally, another relay lens pair is then used to correct the upside-down view. In the OST-HMDs application, it is undesirable to distort the user's FoV through the lenses. $4f$ optics is an optical system used to guarantee that the FoV of the system remains unchanged. However, the viewpoint position's depth is shifted by the lens, so detouring the optical path is required to correct this shift [21].

Moreover, some studies have proposed varifocal optical occlusion. In most occlusion-capable OST-HMDs, the optical depth of the occlusion mask is fixed, resulting in the vergence-accommodation conflict for the occlusion masks [16, 33], similar to that of VR HMDs. Hamasaki et al. physically moved the depth position of the occlusion mask to shift the depth position of the occlusion mask [14]. Conversely, by changing some of the lenses of the $4f$ system to focus-tunable lenses (FTL), Rathinavel et al. realized varifocal occlusion [37]. The former method is limited in durability and driving speed due to the mechanical moving parts. In contrast, the latter approach has a narrow lens aperture and distortion of the user's FoV.

In a subtractive display, a similar lens system is constructed. Its major difference from existing optical occlusion systems is that it requires an optical element that functions as a spatial color filter, rather than a mere black mask as a shielding mask.

Unlike optical occlusion, another branch area of occlusion handling techniques in OST-HMD is the color blending approach [27, 40]. In this approach, an OST-HMD considers the color mixture of the displayed image and the real scene in the user's perspective. A color blending method corrects the displayed colors so that the perceived image fused with a background appears closer to the target image. This approach is more difficult to implement than the optical occlusion approach, because a correct blending requires pixel-precise calibration of the scene and the displayed image. For the processing, a color-calibrated scene camera also needs to synthesize a user-perspective image. More importantly, if the background has colors not included in the displayed image, the method cannot correct it.

2.2 Optical Image Processing

Spatially extracting the desired light from the light in the field of vision has been actively studied in the context of optical image processing (OIP) [2]. In OIP, the SLM achieves the desired optical processing by modulating the amplitude or phase of the input light field passing through the Fourier plane. Shih et al. proposed optical edge enhancement and light addition and subtraction via OIP in polarized systems [38]. They focused the image light on a twisted photosensitive nonlinear liquid-crystal film and achieved edge enhancement by taking advantage of the film's nonlinearity. As a result, only the spatial high-frequency component passes through the system. Although the studies described above feature mainly monochromatic applications, other research has investigated spatial color modulations.

2.2.1 Spatial Color Filtering

Wetzstein et al. proposed a form of OIP using a transmissive color LCD [47]. They built a coaxial $4f$ relay optical system using a scene camera and introduced various perceptual applications in which the color LCD modulates the color of the scene in the FoV. Their applications include contrast enhancement and de-metamerization, that is, separation of perceptually identical colors with different spectral power distributions.

Although their system successfully demonstrated spatial image processing with a transmissive color LCD, there are problems with its use in our application. The biggest problem is that, in principle, transmissive LCDs are unsuitable for subtractive OST-HMDs. As a prerequisite for optical see-through, it is necessary to ensure the visibility of the user's field of vision. In other words, when the display is off, the user's view of the world should be the same as that of the naked eye. However,

in a transmissive SLM, including a transmissive LCD, both pixels and the electrodes that control them are embedded in a transparent substrate, which in principle creates a gap between pixels. Such electrode structures can produce moiré-like artifacts in the perceived image. Above all, the fatal problem is that these microstructures act as passive diffraction gratings, resulting in degraded see-through vision even when the system is turned off. An alternative option is to use reflective LCoS, which is widely used in RGB projectors [28].

2.2.2 Spectral Color Filtering

The use of three primary colors is a universal practice in modern cameras and displays. However, as history demonstrates, the three primary colors are not necessarily the only absolute color representation principle: at the dawn of color photography in the 19th century, Lippmann invented natural color photography, that is, photography that records light across a broad visible light band [31, 34]. The natural color photography developed by Lippmann uses light interference. It uses a thin, nearly transparent photographic emulsion containing silver halide particles and a temporary mirror of liquid mercury to record interference by standing waves at the reflective surface of the incident light.

Harm et al. combined PSLM and white illumination to produce full-color images without RGB color masks [15]. Their method essentially searched for multispectral colors even though they measured colors in a standard three-color space via a CMOS camera. The reflective design also has advantages over the transmissive SLM design, such as improved color efficiency and spatial resolution. However, their system lacked an explicit intensity modulation, except as a by-product of the birefringence effect. Driencourt et al. proposed a tunable color filter with a wide color gamut by mixing birefringent-induced colors from a liquid crystal cell and a plasmonic nanostructure–subwavelength nanostructures [9]. Combining a patterned polarizer, they demonstrated full-color image generation.

The study by Itoh et al. mentioned in the introduction gave a detailed analysis of these phase modulation color approaches. Their design was dedicated to a single-PSLM setup and focused on realizing it as a proper optical see-through display [17]. However, the color range on the color gamut was somewhat limited.

3 METHOD

3.1 Color Filtering with a Single PSLM

First, we briefly introduce the mechanism of color filtering using a single PSLM [17]. PSLM is a type of liquid crystal device that provides a variable amount of phase shift (retardation) between p- and s-polarization by rotating liquid crystal molecules. The color filter utilizes the PSLM placed between two orthogonal linear polarizers to modulate the transmittance of the incoming light over the wavelength. For the analysis of the color filter, we introduce the Jones calculus [29], which can model the polarization state's behavior as a linear calculation.

Fig. 2 shows an overview of how the unpolarized light of a particular wavelength is modulated by the combination of a PSLM and polarizers. Light is electromagnetic waves that oscillate in random directions. When such oscillations are limited to a particular direction or rotation at a constant rate in a plane, the light is referred to as polarized. Suppose that a monochromatic plane wave of light is traveling in the positive z-direction, with angular frequency ω and wave-number $k = \omega/c$. Then, we denote the x and y components of the complex amplitude of electric fields $\mathbf{E}(z, t)$ at z and time t as follows:

$$\begin{aligned} \mathbf{E}(z, t) = \begin{bmatrix} E_x(z, t) \\ E_y(z, t) \end{bmatrix} &= \begin{bmatrix} E_{0x}e^{-i(kz-\omega t+\phi_x)} \\ E_{0y}e^{-i(kz-\omega t+\phi_y)} \end{bmatrix} \\ &= e^{-i(kz-\omega t)} \begin{bmatrix} E_{0x}e^{-i\phi_x} \\ E_{0y}e^{-i\phi_y} \end{bmatrix} \end{aligned} \quad (1)$$

The vector $[E_{0x}e^{-i\phi_x}, E_{0y}e^{-i\phi_y}]^T$ in Eq. (1) is called the Jones vector; it represents the amplitude and phase of the electric field in the x and y directions. In particular, when the light is represented by a combination of components of light parallel or perpendicular to the incident angle of a given linear polarizer, each component is referred to as p-polarized

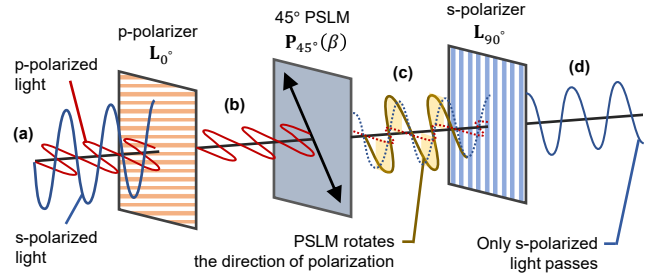


Fig. 2. Overview of Color Filtering with a PSLM and Polarizers. (a) The unpolarized incident light $\mathbf{E}(z, t)$ consists of a p- (red) and s-polarized (blue) component. (b) When this unpolarized light enters the p-polarizer \mathbf{L}_{0° , only the p-polarized light passes through it. If the p-polarized light directly enters the s-polarizer \mathbf{L}_{90° , which has an orthogonal polarization angle, the incident light is completely occluded. (c) Because the PSLM $\mathbf{P}_{45^\circ}(\beta)$ can rotate the direction of polarization of the incident light by an angle β , the direction of p-polarization can be rotated by placing the PSLM behind the p-polarizer (yellow). (d) As a result, the rotated polarized light is again decomposed into p- and s-components, and the s-polarized component can pass through the s-polarizer \mathbf{L}_{90° .

and s-polarized light, respectively. For the sake of simplicity, the Jones vector is commonly normalized to 1 at the start of the calculation.

Similarly, the Jones matrix is an operator representing the polarization of light as it passes through an optical element, such as a lens, beam splitter, or mirror. Using the Jones matrix, the ideal linear polarizers with horizontal (p-polarized, 0°) and vertical (s-polarized, 90°) transmission axes can be denoted as \mathbf{L}_{0° and \mathbf{L}_{90° , respectively:

$$\mathbf{L}_{0^\circ} = \begin{bmatrix} 1 & 0 \\ 0 & 0 \end{bmatrix}, \quad \mathbf{L}_{90^\circ} = \begin{bmatrix} 0 & 0 \\ 0 & 1 \end{bmatrix} \quad (2)$$

A Jones matrix of the PSLM \mathbf{P} can also be termed a dynamic phase retarder [49, 50]:

$$\mathbf{P} = e^{-i\phi} \begin{bmatrix} e^{-i\beta} & 0 \\ 0 & e^{i\beta} \end{bmatrix} \quad (3)$$

where

$$\beta(\lambda, m) = 2\pi n(m)d/\lambda. \quad (4)$$

Moreover, $n(m)$ is the refractive index of liquid crystals in the x-axis of each pixel on the PSLM, and m is the input value to the PSLM pixel. For example, if the PSLM employs an 8-bit input, then $m = 0, \dots, 255$. Further, d is the thickness of the liquid crystal layer, and λ is the wavelength incoming into the PSLM. From the above, we see that PSLMs modify the retardance β and control the ratio of x and y components of the output light while maintaining its amplitude. Note that the retardance β depends on the input value to the PSLM pixel m and the wavelength of the incoming light λ . For convenience, we ignore the term of general phase shift $e^{-i\phi}$ in the following discussion.

When an optical element \mathbf{M} in the Jones matrix is rotated axially, the Jones matrix \mathbf{M}_θ after rotation is

$$\mathbf{M}_\theta = \mathbf{R}^T(\theta)\mathbf{MR}(\theta), \quad \text{where } \mathbf{R}(\theta) = \begin{bmatrix} \cos(\theta) & \sin(\theta) \\ -\sin(\theta) & \cos(\theta) \end{bmatrix} \quad (5)$$

To use a PSLM \mathbf{P} as a polarized color filter, the PSLM is first rotated 45° and then combined with linear polarizers with angles of 0° and 90° . As a result, the Jones matrix of the single polarized color filter \mathbf{C}_1 can

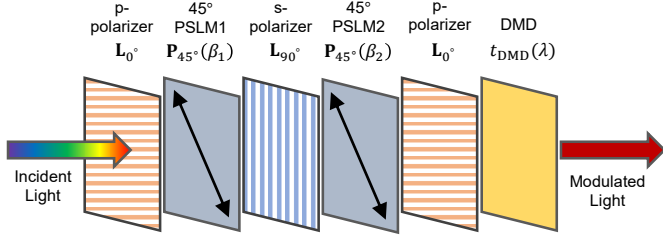


Fig. 3. An optical scheme and the Jones matrices of the color filter using cascaded PSLMs and polarizers. Note that in this figure, PSLMs appear transmissive only for explanatory purposes; our system does use reflective PSLMs.

be denoted as follows:

$$\begin{aligned} \mathbf{C}_1(\beta) &= \mathbf{L}_{90^\circ} \cdot \mathbf{P}_{45^\circ}(\beta) \cdot \mathbf{L}_{0^\circ} \\ &= \begin{bmatrix} 0 & 0 \\ 0 & 1 \end{bmatrix} \begin{bmatrix} \cos(\beta) & -i\sin(\beta) \\ -i\sin(\beta) & \cos(\beta) \end{bmatrix} \begin{bmatrix} 1 & 0 \\ 0 & 0 \end{bmatrix} \\ &= \begin{bmatrix} 0 & 0 \\ -i\sin(\beta) & 0 \end{bmatrix} \end{aligned} \quad (6)$$

Finally, transmittance t , the ratio of the intensity of output light to input, is given by the absolute value of the complex amplitude over the wavelength λ :

$$t(\lambda, m) = \|\mathbf{C}_1\|_2 = \sin^2(\beta(\lambda, m)) \quad (7)$$

This equation shows that the transmittance over the visible wavelength varies with the value of the PSLM m ; that is, the optics can make 256 color filters when the PSLM has the 8-bit inputs.

3.2 Color Filtering with Cascaded Multiple PSLMs

Eq. (7) implies that each color filter has broad color bands and several peaks over the visible light band. As a result, the color space where all color filters can display is smaller than conventional RGB displays. A possible solution for making a color filter narrower is cascading multiple phase retarders [1]. In this section, we explain the Jones calculus of the color filters using multiple PSLMs.

The simplest configuration of the color filters with multiple PSLMs is that p- and s-polarizers are placed alternately. The PSLMs are inserted between each polarizer, as shown in Fig. 3. We now assume that N PSLMs are cascaded, and we then denote the phase retardation and Jones matrix on the i -th PSLM ($i = 1, \dots, N$) as $\beta_i = 2\pi n(m_i)d/\lambda$ and $\mathbf{P}(\beta_i)$, respectively. In this case, the Jones matrix of the cascaded multiple PSLMs \mathbf{C}_N can be denoted as follows:

$$\begin{aligned} \mathbf{C}_N(\beta_1, \dots, \beta_N) &= \mathbf{L}_{0^\circ} \cdot \mathbf{P}_{45^\circ}(\beta_N) \cdot \mathbf{L}_{90^\circ} \cdot \mathbf{P}_{45^\circ}(\beta_{N-1}) \\ &\quad \cdots \mathbf{L}_{90^\circ} \cdot \mathbf{P}_{45^\circ}(\beta_1) \cdot \mathbf{L}_{0^\circ} \end{aligned} \quad (8)$$

For instance, the Jones matrix of the color filter \mathbf{C}_2 in $N = 2$ can be denoted as follows:

$$\begin{aligned} \mathbf{C}_2(\beta_1, \beta_2) &= \mathbf{L}_{0^\circ} \cdot \mathbf{P}_{45^\circ}(\beta_2) \cdot \mathbf{L}_{90^\circ} \cdot \mathbf{P}_{45^\circ}(\beta_1) \cdot \mathbf{L}_{0^\circ} \\ &= \begin{bmatrix} 1 & 0 \\ 0 & 0 \end{bmatrix} \begin{bmatrix} \cos(\beta_2) & -i\sin(\beta_2) \\ -i\sin(\beta_2) & \cos(\beta_2) \end{bmatrix} \begin{bmatrix} 0 & 0 \\ -i\sin(\beta_1) & 0 \end{bmatrix} \\ &= \begin{bmatrix} -\sin(\beta_1)\sin(\beta_2) & 0 \\ 0 & 0 \end{bmatrix} \end{aligned} \quad (9)$$

As a result, transmittance $t_N(\lambda)$ is given over the wavelength λ and the pixel values $\{m_i\}_{i=1}^N$ on each display:

$$t_N(\lambda, \{m_i\}_{i=1}^N) = \|\mathbf{C}_N\|_2 = \prod_{i=1}^N \sin^2(\beta_i(\lambda, m_i)) \quad (10)$$

The number of color filters of the cascaded PSLMs is equal to the number of combinations of $\{m_i\}_{i=1}^N$. For example, if PSLMs accept 8-bit inputs and we use two PSLMs (i.e. $N = 2$), the number of color filters is $256^2 = 65536$.

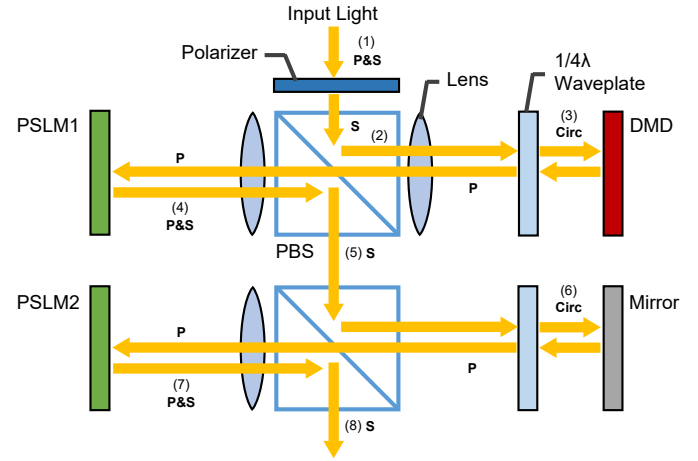


Fig. 4. Schematic of the optical design of a cascading see-through system. The incident light from the world enters the relay lens system through the SLMs to the eye.

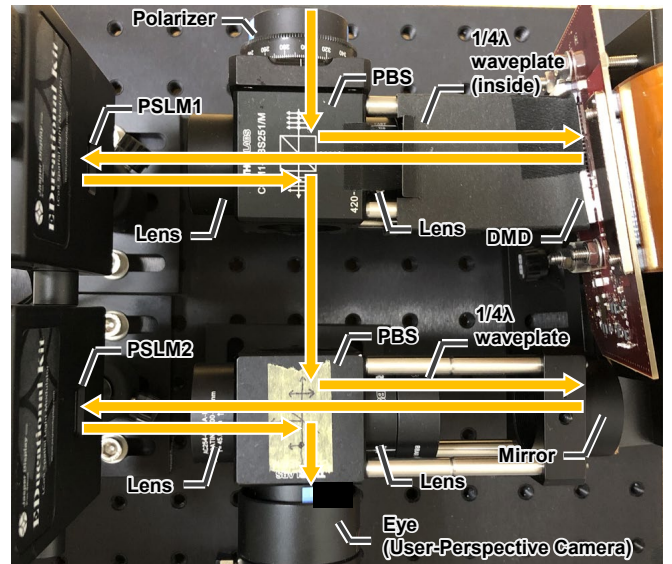


Fig. 5. Hardware setup of our experiment. The schematic is identical to Fig. 4.

3.3 Amplitude Modulation for an Arbitrary Light Input

An amplitude spatial light modulator, such as DMD, modulates the amplitude of the incident light by $t_{DMD}(\lambda, m_D)$ according to the input m_D . Because the amplitude modulator does not affect the polarization states, we can multiply $t_{DMD}(\lambda, m_D)$ by the transmittance of the color filter to calculate the transmittance of the entire system. Thus, when we denote the spectrum of the incident light as $e(\lambda)$ and $N = 2$, the filtered spectrum after passing through the system, $o_2(\lambda)$, can be calculated as follows:

$$o_2(\lambda, m_1, m_2, m_D) = e(\lambda) t_2(\lambda, m_1, m_2) t_{DMD}(\lambda, m_D) \quad (11)$$

4 IMPLEMENTATION

In this section, we first present the optical design and the hardware setup of the system. We then describe the calibration of the PSLMs, which is essential to optimizing the color filter performance.

4.1 Optical Design

Our StainedView system extends the optical design of LAD [17] to cascade two PSLMs and a DMD while keeping the system see-through

without dramatically shifting the viewpoint.

In our system, a polarized beam splitter (PBS) makes each PSLM function as a color filter. A PBS is a cubic optical element that splits the unpolarized incident light into p-polarized and s-polarized light. The former passes through the PBS, whereas the latter exits from the side of the cube by reflected 90°. Due to the PBS in front of a PSLM, the p-polarized light enters the PSLM. The PSLM modulates the light and reflects it. The reflected light again enters the PBS and splits into p-polarized and s-polarized light. The outgoing s-polarized light is the color-filtered light. Fig. 3 shows these optical processing steps.

A DMD consists of microscopic flipping mirrors. Thus, it modulates only the amplitude of the incident light and does not change the phase of the light. Because the input light for the DMD in our setup is s-polarized, the output light cannot pass through the PBS. Thus, we place a quarter-wave ($\lambda/4$) plate in front of the DMD to swap the polarization states of the input light.

In addition, we place lenses with the same focal length in front of each PSLM to focus the image plane on it. The resulting color filter appears as a 2D layer at a fixed distance (typically infinity) in the user's FoV.

Figure 4 shows a schematic of the optical design of our system and the light paths passing through it. First, (1) the unpolarized incoming light passes through a linear polarizer and becomes s-polarized. (2) The s-polarized light is then reflected by 90° on the PBS and enters the DMD. (3) The DMD modulates the amplitude of the light, and the $\lambda/4$ plate makes the output light p-polarized. This p-polarized light passes through PBS and reaches PSLM1. (4) The p-polarized light is phase-modulated on PSLM1 and becomes both p- and s-polarized. (5) This unpolarized light splits again on the PBS. The s-polarized component is reflected by 90° and enters the next PBS. In the same manner, the light is then reflected by (6) the mirror and (7) PSLM2. Finally, (8) the output is the s-polarized component reflected by PSLM2.

Note that the p-polarized component of the light reflected by PSLM2, which is separated in (8) but does not reach the eye, is reintroduced to PSLM1 by reversing the existing optical path, which causes second-order reflections. Although this loop-back is attenuated by increasing the number of optical elements between PSLM1 and PSLM2 in the current system, it causes deterioration of our color filters. The effects of the second-order reflection are discussed in detail in Sec. 5.3.

4.2 Hardware Setup

Following Fig. 1 (a), Fig. 5 shows our hardware setups. For the DMD and its controller, we used a DLP LightCrafter 6500 from Texas Instruments (1920 × 1080 pixels). For the PSLM, we used two Jasper Display EDK 9554 A+ (1920 × 1080, 60 Hz). In the PSLM, the phase shift of each pixel can be linearly controlled by 8-bit inputs. These PSLMs and the DMD are connected to a laptop by an HDMI interface via the controller. Other components were from Thorlabs: LPVISE100-A for linear polarizers, AQWP10M-580 for the achromatic 1/4 waveplates, PBS251 for the PBS, BB1-E02 for the mirror, and AC254-045-A for the lens. We installed a XIMEA MC031CG-SY-UB (2064 × 1544 pixels) as the user-perspective camera and set its gamma value to 1/2.2.

4.3 Parameter Estimation for PSLMs

Analogously to the color calibration of ordinary displays, calibration of the retardance (phase-shift) responses of a PSLM improves the accuracy of the color filter analysis. Before the simulation of the color filters obtained by StainedView, we thus measure the retardance output $\beta_i(\lambda, m_i)$ of each PSLMi ($i = 1, 2$) for a given input 8-bit value m_i in the following manner.

From Eq. 4, the retardance β_i is inversely proportional to λ ; we thus approximate β_i with a linear function,

$$\beta_i(\lambda, m_i) = \frac{2\pi}{\lambda} (A_i m_i + B_i), \quad (12)$$

and estimate A_i and B_i by comparing β_i with measured filters.

We estimated these parameters as follows. First, we built a setup to configure a color filter with a single PSLM; that is, we built only the lower part (5)-(8) in Fig. 4.

Next, we placed a white light source in front of the system. We displayed uniform phase images from 0 to 255 (256 images in total) and measured the spectra of the output light with a spectroradiometer (UPTek MK350N Premium). As a reference light source, we used a Thorlabs SOLIS-3C High-Power LED 5700K (Day Light White) with a DC2200 High-Power 1-Channel LED Driver. Fig. 7 shows the spectrum of the light source as measured by a spectroradiometer (UPTek MK350NPremium), which has a measurement range from 380 to 780 nm with a measurement step of 1 nm.

After capturing the 256 measurements, we computed each color filter. The color filters were subsequently divided by both the base illumination spectrum (Fig. 4) and the transmittance spectrum of each optical element specified in their datasheets, discussed below in Sec. 5.2. We then obtained the wavelength-dependent transmittance of the PSLM itself:

$$t(\lambda, m_i) = \sin^2(\beta_i(\lambda, m_i)). \quad (13)$$

Finally, the parameters A_i and B_i of Eq. 12 were obtained by curve fitting using the least-square method, assuming that $t(\lambda, m_i)$ follows a $\sin^2(\cdot)$ curve.

As a result of the measurements, we estimated the parameters of each PSLM as follows:

$$\beta_1(\lambda, m_1) = \frac{2\pi}{\lambda} (1.005m_1 + 563.664) \quad (14)$$

$$\beta_2(\lambda, m_2) = \frac{2\pi}{\lambda} (1.078m_2 + 515.175) \quad (15)$$

Note that the PSLMs we used are designed for $\lambda = 532$ nm.

5 SIMULATION

In this section, we describe a simulation of the color filter characteristics of a dual-PSLM system. First, we simulate the color filters under the ideal environment. Then we compute the color response under the white light source used in the experiment (Sec. 5.1). In an actual system, each optical element attenuates the incident light according to the wavelength (Sec. 5.2), and the color filter degrades due to secondary reflections in the system (Sec. 5.3). By performing a simulation that takes these factors into account, we can obtain a color response that is closer to the actual system.

5.1 Filter Benchmarks

5.1.1 Basic Color Filters of the Dual-PSLM Setup

We firstly simulate the filter performance in the basic dual-PSLM setup described in Sec. 3.2. Fig. 6 shows (a) simulated-color filters under a single-PSLM setup, (b) simulated-color filters of the dual-PSLM setup of some given phase values. We calculated the simulated color filters via Eq. (10) using the retardance parameters obtained in Sec. 4.3.

Compared to the single-PSLM color filters, the dual PSLMs have a narrower bandwidth for each filter. Thus, the color filter can express more pure colors that are closer to a single-wavelength light. Moreover, the color filters of each PSLM can be multiplied to complement different bandwidths, enabling the expression of colors that cannot be achieved with a single PSLM.

For a more qualitative evaluation of the performance, we mapped each color filter on the $u'v'$ color space via CIE 1976 $L^*u^*v^*$ standard colors (Fig. 6, (c)). The figure shows that the color filters of the dual PSLMs (gray) cover a wider color gamut than those of the single PSLM (PSLM1-only, yellow). Furthermore, the color filters of the dual PSLMs cover a wider color range for greenish color compared to the sRGB (black triangle) color space, a common color standard reproduced by conventional RGB displays.

Whereas the color filters of the single PSLM can represent only 256 color points on a curve, the dual PSLM can cover 65,536 colors as a surface. The sparse color points also require a trick to depict a target color. In LAD [17], they applied a Delaunay triangulation on the color space to search a triangle for a target color. Then they time-multiplexed the corresponding three phase values (m) to represent the target color.

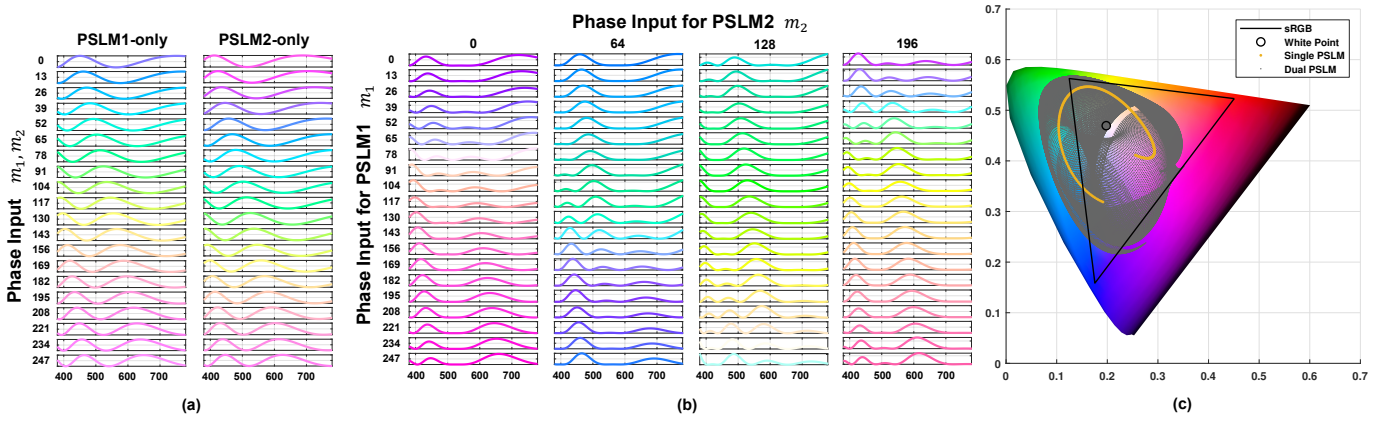


Fig. 6. An overview of the color-filter simulation of both the single-PSLM and the dual-PSLM setups without intensity modulation by the DMD. (a) Some filters in the spectrum domain for the single-PSLM setup and (b) for the dual-PSLM setup. (c) Color filter spectra are converted into the XY colors and plotted on the color gamut. Overall, our dual-PSLM setup considerably improves the color range of the single-PSLM setup.

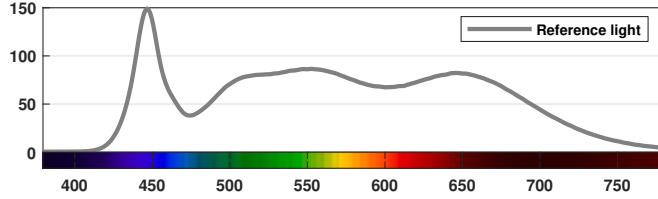


Fig. 7. The spectrum of the reference light we used for all calibrations and experiments. The x-axis is the wavelength, and the y-axis is the irradiance [mW/m^2].

This time-multiplexing requires a higher number of frames to get closer to the target color, resulting in a lower frame rate. In our dual-PSLM setup, on the other hand, the sample points in the color space are so dense that it is sufficient to choose a combination of points (m_1, m_2) that are close to the target color. It leads to faster image processing and a higher frame rate.

Fig. 9 shows the changes in the intensity and color of the color filter for each combination of (m_1, m_2) . As this figure illustrates, the intensity is brighter when m_1 and m_2 are close to $\beta_1(m_1) = \beta_2(m_2)$ and darker when $|\beta_1(m_1) - \beta_2(m_2)| = \pi$. In determining the value of DMD, the intensity attenuation caused by the dual PSLMs needs to be taken into account.

5.1.2 Color Responses with External Light

The color space that our system can achieve depends on the input light spectrum. Because the color filters computed in the previous section were derived under the uniform input light spectrum, we can easily update the new color responses given an input spectrum. Throughout the remaining simulations and experiments, we use the reference light shown in Fig. 7 as the standard input light, if not otherwise specified. The color gamut in Fig. 8 (b) shows the color response with the reference light. Because the reference light has a strong blue band in the spectrum, the color response is more towards the blue side than the color filters with the uniform light in Fig. 8 (a).

Be aware that the lighting condition of a scene also affects human color perception. Thus, looking at the color distribution of the system only under a certain input light source does not guarantee the presentation of wide-color sensations. Although this perceptual investigation is beyond the scope of this study, it is an important research topic that requires further study.

5.2 The Transmittance of Each Optical Element

In the previous section, the color response was computed based on the assumption that all optical elements allow 100% of light to pass

through. In practice, however, optical elements attenuate light according to wavelength. In this section, we compensate for the color gamut computed in the previous section by multiplying the optical system's transmittance based on the catalog specifications.

We denote the transmittance of the polarizer as $t_{\text{pol}}(\lambda)$ and the transmittance of the waveplate as $t_{\text{wav}}(\lambda)$. Also for PBS, we denote the transmittance of p-polarized light and the reflectance of s-polarized light as $t_{\text{PBS}}(\lambda)$ and $r_{\text{PBS}}(\lambda)$, respectively. According to Eq. (11) and Fig. 4, the output spectrum with transmittances of optic parts $o'(\lambda)$ can be computed as follows:

$$\begin{aligned} o'(\lambda) &= r_{\text{PBS}}^4(\lambda) t_{\text{PBS}}^2(\lambda) t_{\text{wav}}^4(\lambda) t_{\text{pol}}(\lambda) o_2(\lambda) \\ &= t_{\text{all}}(\lambda) o_2(\lambda) \end{aligned} \quad (16)$$

where $t_{\text{all}}(\lambda)$ is the products of the transmittance of all the optical elements. Fig. 10 shows $t_{\text{all}}(\lambda)$ of our hardware setup.

Fig. 8 (c) shows the color gamut that the system can represent after taking into account the transmittance of the optical elements. Due to the large attenuation of transmittance $t_{\text{all}}(\lambda)$ in the short wavelength range, the corrected color gamut is more towards the red compared to Fig. 8 (b).

5.3 Second-order Reflections between PSLMs

In our setup, each PBS is regarded as the p- and s-polarizer sandwiching each PSLM. As a result, when the light from PSLM2 is separated into p- and s-polarized light, the separated p-polarized light, which needs to eliminate, re-enters PSLM1 and causes higher-order reflections (Fig. 11). This loopback due to higher-order reflections should be taken into account for more accurate simulations.

Here, we consider only second-order reflections. From the light path illustrated in Fig. 11 (orange and gray), the transmittance of the loopback $t_{\text{lb}}(\lambda)$ and output spectrum that compensates for the second-order reflections $o''(\lambda)$ can be calculated as follows:

$$t_{\text{lb}}(\lambda) = r_{\text{PBS}}^4(\lambda) t_{\text{PBS}}^2(\lambda) t_{\text{wav}}^4(\lambda) \quad (17)$$

$$o''(\lambda) = \frac{1}{1 - t_{\text{lb}}(\lambda)} o'(\lambda) \quad (18)$$

Fig. 8 (d) shows the color gamut that compensates for the second-order reflections.

6 CALIBRATION

6.1 Deviation of PSLM Values from Actual Measurements

Theoretically, the combined transmittance of PSLM and PBS as described in Sec. 3.1 should be $\sin^2(\beta)$, but our actual measurement showed strained waveforms. In the experiment, we measured the spectral transmission of each PSLM for all input values (0–255) with the

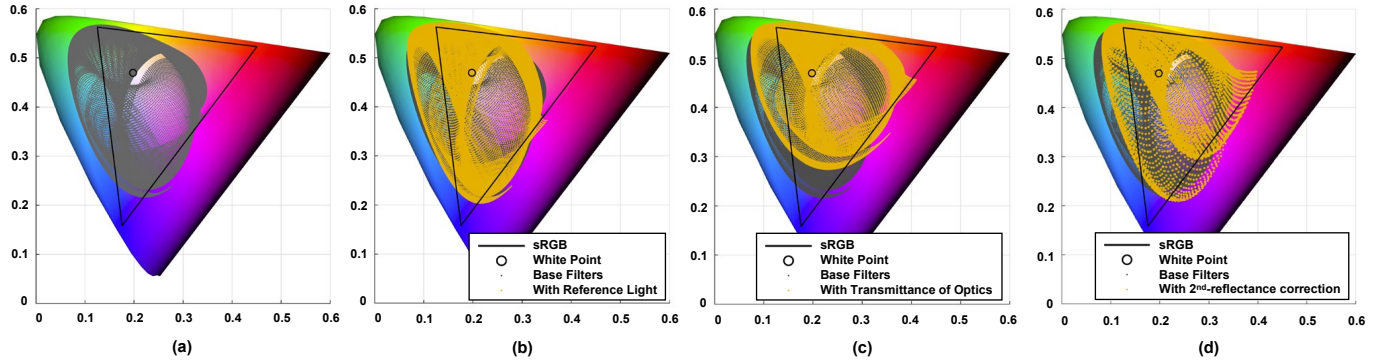


Fig. 8. Simulations of the color filters under different input light spectra. (a) Colors under the uniform light source (b) Colors under the reference light spectrum (Fig. 7). (c) Colors updated (b) with the transmittance of all optical components (r_{all} in Eq. 16) in the prototype considered. (d) Improved colors of (c) with the second reflection considered.

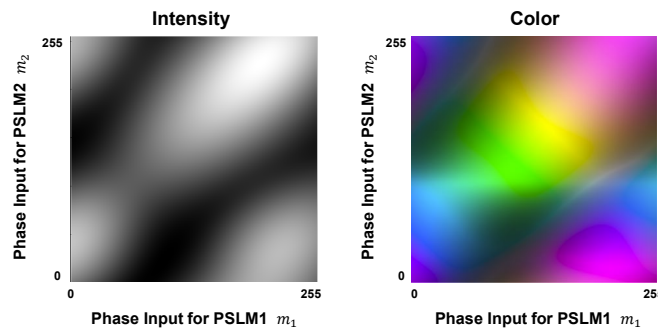


Fig. 9. Visualization of the simulation of the color filters for all phase combinations in the dual-PSLM setup without the DMD modulation. (left) Intensity-only map induced by the color filters (right) Color map converted into the RGB color space.

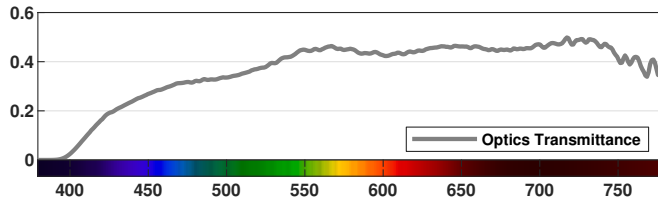


Fig. 10. The overall transmittance of the prototype based on the datasheets of the passive optical components (r_{all} in Eq. 16)

reference light source in advance. Using the transmittance multiplied by the wavelength-specific transmittance of the other optics (values in the datasheet for each component), we created a look-up table of the spectral transmission for the entire system.

6.2 Pixel-wise Mapping between Displays

For the spatial correction, we needed to warp the input images to the DMD and PSLMs so that they are aligned from the user's perspective. To achieve this, we used a gray code pattern to obtain the pixel correspondences between the user-perspective camera and each display. We then estimated homographies from the camera to the displays and corrected the input images based on them.

7 VERIFICATION AND DEMONSTRATION

Following the intensive benchmark of the StainedView system in the previous simulation section, in this section, we verify the simulation results and also demonstrate the color performance of the StainedView system, showcasing some examples of images.

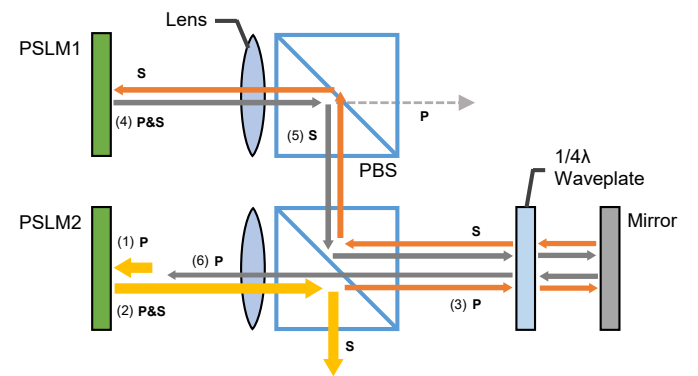


Fig. 11. Conceptual illustration of the second-order reflection. (Sec. 5.3). (1) The p-polarized light entering PSLM2. (2) It becomes p- and s-polarized light and is divided into p and s in PBS. (3) The p-polarized light reverses the orange path and returns to PSLM1. (4) After running in reverse, it is further reflected by PSLM1 and becomes p&s. (5) In PBS, p- and s-polarized light are separated, and the s-polarized light follows the gray path. (6) It enters the PSLM2 again via the forward route (gray).

7.1 Color Filter Comparison

We first evaluate the performance of the individual color filter quantitatively for a given phase value pair for the two PSLMs. We displayed a single-phase image of the size 256×256 on the PSLMs and then measured with the spectrometer.

Fig. 13 shows a comparison between the actual measurement and simulation. The measurement showed that our system can represent 75.8% of the sRGB color space under the reference light, compared to 41.4% for LAD [17]. Hence, we confirmed that the additional PSLM effectively increases the color range.

The experiment also showed that the actual measurement and simulation are close to each other; thus, we confirmed that our simulations and calibration procedure roughly reproduced the color filters and color responsiveness of our system. However, the input values and color mapping details did not match, with the maximum difference between the measurement and simulation being 0.137 in the UV color space. We provide a discussion of this discrepancy in Sec. 8.2.

7.2 Color Chart and Teapot

This benchmark qualitatively tests the color fidelity of the display by displaying sample images: the Macbeth color chart and a color Utah teapot. To evaluate the maximum performance of the system, we generated input images by referencing the color table created from the measured data shown above. Fig. 12 summarizes the result. As an example of input images, Fig. 14 shows input images used for the

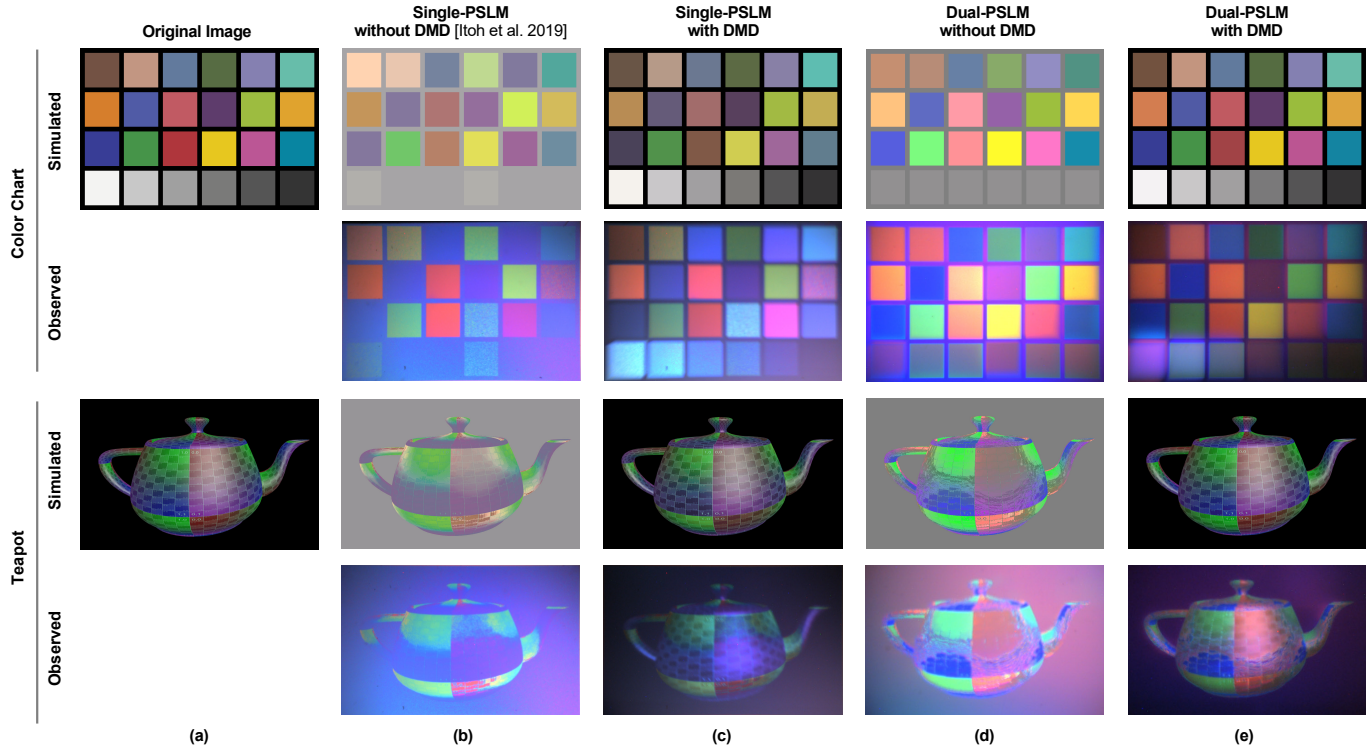


Fig. 12. Formation of images by the system with a reference light source. We set the phase-image frame division for time-multiplexing image formulation in the single-PSLM setup to 10.

dual-PSLM setup for the teapot.

The single-PSLM setup of LAD [17] can neither faithfully reproduce the target color due to the narrow gamut nor manipulate chromaticity and brightness independently. By contrast, our single-PSLM + DMD setup suppresses the excessive brightness of the reddish cells and provides accurate grayscale contrast representation at the bottom of the color chart. The yellow cells, however, become bluish due to the narrower color gamut of the single-PSLM setup. On the other hand, the dual-PSLM + DMD setup has a wider color gamut and produces accurate colors except for the faded red cells in the color chart.

However, due to the gaps around each micromirror of DMD, the space around the cells of the color chart and teapot are not completely black, but a little reddish. Furthermore, the outer cells of the color chart in Fig. 12 (e) have color bleeding due to the misalignment between DMD and PSLM images. This is because we calibrated the displays without regard to lens distortions, as mentioned in Sec. 6.2.

Furthermore, using a more practical AR scenario, we demonstrated the system in a see-through subtractive AR setup. We displayed the Utah teapot on the system with a background with a table. Fig. 1(d) shows the results. One can see that the virtual, opaque-looking teapot is merged into the table scene.

8 DISCUSSION AND PROSPECTS

In this section, we investigate the current system's remaining issues and discuss the prospects for future research on subtractive OST displays.

8.1 Optics: Occlusion, Focus, and FoV

In our prototype, we used a DMD for intensity modulation. The DMD, however, is not necessarily the best option for intensity modulation due to its 45-tilted mirror axis and its positive and negative mirror tilt angles. Other modulation approaches, such as with LCOS displays [5, 48], could be effective alternatives.

Similar to existing OST-HMDs, our subtractive image is focused at a fixed focal distance. As mentioned in the related work section, our optics shares much optical design with occlusion-capable OST-HMDs.

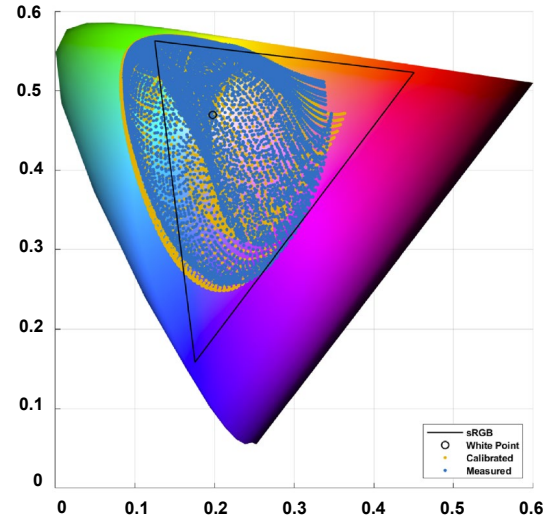


Fig. 13. Comparison between the simulation and the observation with the reference light. (yellow) the color gamut of the color filter obtained by our simulation and calibration. (blue) the actual measured gamut.

Thus, their knowledge on making occlusion masks varifocal can be transferred to our system [14, 37].

The narrow FoV is also an issue that needs to be addressed. In particular, the addition of a DMD and an additional PSLM in our system increases the optical path length and narrows FoV compared to LAD [17]. Essentially, a sophisticated waveguide approach coupled with the relay optical system embedded in the optical path is necessary. The development of such optics is a challenging design task, but a means of overcoming this challenge may lie in recent compact near-eye display design with beam combiner coatings embedded inside the

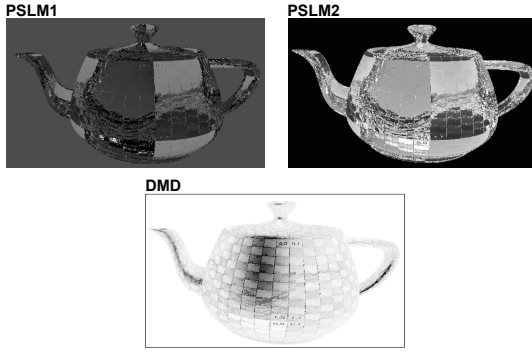


Fig. 14. The input phase and opacity images used for the teapot image in Fig. 12.

waveguide [19].

8.2 Errors in the Simulations

As mentioned in Sec. 7.1, our color simulations and calibrations are still not perfectly consistent with actual observation. This discrepancy may stem from ignoring the fact that the amount of retardation caused by a PSLM is dependent on the incident light's wavelength. The current model also ignores the effect of the temperature of the environment on the retardation amount. Incorporating wavelength-dependent gain and temperature-dependent phase shift may improve the simulation.

8.3 Transmittance

In our prototype, the luminosity of the incoming outside light is attenuated by half by the polarizing optics. Each optical element further darkens the user's field of view.

Our simulation showed that the transmittance is about 0.7–11.6% (avg. 5.1%) under the reference light, depending on the spectrum of incoming light on the current prototype. Our simple measurement of Hololens 2 transmission showed that it is around 31–37%, depending on the incident angle of the spectrometer.

Even though human vision is logarithmic, this transmission should be improved. On the engineering side, developing higher transmittance optical elements and higher reflectance PSLMs could solve the problem. Enlarging the aperture of the system is another possible solution.

8.4 Color Optimization

Our system achieved a much wider color gamut than the existing method. However, our prototype did not cover the entire sRGB color gamut. Cascading more PSLMs would certainly help to increase the color range, yet it is not the best solution given the increase of the complexity of the optics and the loss in transmittance. In addition to research on the liquid crystal element, studies have explored expanding the color gamut by combining a special polarization layer [9]. Exploring such optical improvements would be one of our options.

Another observation in our system was the secondary reflections occurring in our optics. Secondary reflections are not a problem if the only objective is to simulate the properties of the color filter. However, in terms of improving color reproduction capability, secondary reflection is problematic, because it causes the color filter to lose its sharpness. For practical purposes, a mechanism for preventing such unwanted reflections would be necessary.

At a more microscopic level, any high-resolution liquid crystal devices, including LCoSs and transmissive TFT LCDs, suffer from the fringing field effect, a form of cross-talk between adjacent pixels [6, 10]. When different voltages are applied on adjacent pixels, the liquid crystal molecules near the pixel edges are distorted by the lateral component of the fringe field, significantly degrading the electro-optical performance of the device. In PSLMs, the effect appears as a phase-values disturbance at the pixel boundaries. Some works from the holography community have proposed methods for alleviating the fringing field

effect by taking the cross-talk into account in their phase image optimizations [30, 36]. This knowledge can be transferred to our phase estimation algorithm.

8.5 Beyond Liquid-Crystal-Based SLMs

Although we have explored subtractive displays with PSLM, this approach is bounded by the physical limitation of liquid crystal devices in terms of pixel pitch size (a few microns) and light efficiency. Beyond the liquid crystal approach, in optical engineering, extensive efforts have been devoted to light modulation using various subwavelength structures known as metasurfaces [18, 32]. Metasurfaces have attracted a great deal of interest due to their exotic optical and electromagnetic properties, which never appear in ordinary materials. One application of metasurfaces is as color materials, because they can realize extremely high light efficiency and good color properties with submicron resolution. Examples of such realizations include diffraction gratings [39, 51], plasmonic nanostructure dots [42, 45], metasurfaces [8]. Although the typical metasurface is static *printed*, some research groups have sought tunable metasurfaces [7, 44]. Spin-SLM is an alternative active SLM with a submicron pitch that uses the magneto-optical effect [3].

8.6 Combining Additive OST-HMDs

A subtractive AR display is complementary to an additive AR display in its functionality [17]. If we can combine additive and subtractive AR displays, doing so will increase the flexibility of the AR images and the environment in which they can be used. In addition, considering the rise of studies on autofocus eyeglasses [35], the integration of these studies may enable optical image processing to augment human vision directly to assist it.

The simplest way to build an additive-subtractive AR display is to add subtraction optics as an add-on to an existing additive display, but for obvious reasons this is not a good idea. In essence, we think it is reasonable to follow the optical design of occlusion-capable OST-HMD and replace the SLM for amplitude modulation with a PSLM and incorporate polarization optics.

8.7 Hardware Miniaturization

As shown in Fig. 5, our prototype is still large and bulky. We believe that the designs of some existing occlusion-capable OST-HMDs can be helpful for miniaturization. For example, folded optics would be helpful for our setup. Miniaturization would also be achieved by engineering advances such as improvements of optical devices.

8.8 Other Applications

Modulating white light with PSLMs has also inspired applications in projectors [25] and displays [15]. Because our system gives colors with color spectra, we can apply our optics to hyperspectral imaging and projectors.

9 CONCLUSION

We presented StainedView, a subtractive optical see-through full-color display with intensity modulation capability. The system is superior to the current work, with a 1.8 times wider color range (75.8% fulfillment of sRGB color space versus 41.4%) and the capacity of the color filters to achieve variable intensity. Our optical see-through design employs mainly cascaded PSLMs and a DMD. Thanks to the cascaded PSLMs, we can expand the color gamut of the spatial color filter. We also provided a thorough end-to-end analysis of how a broadband light propagates through our polarized optical system, which allowed us to simulate the complex nature of the color filters and to develop an optimized color rendering algorithm. With a proof-of-concept system, we verified that our method achieved the aforementioned performance and demonstrated its uses in a typical AR scenario. We hope this study encourages researchers to explore the potential of subtractive AR displays and enhance the visual AR experience.

ACKNOWLEDGMENTS

This study was supported by JST PRESTO Grant Number JPMJPR17J2 and JSPS KAKENHI Grant Number JP20H04222, Japan.

REFERENCES

- [1] O. Aharon and I. Abdulhalim. Liquid crystal lyot tunable filter with extended free spectral range. *Opt. Express*, 17(14):11426–11433, 2009.
- [2] A. Alfalou and C. Brosseau. Recent advances in optical image processing. In *Progress in optics*, volume 60, pages 119–262. Elsevier, 2015.
- [3] K. Aoshima, H. Kinjo, K. Machida, D. Kato, K. Kuga, T. Ishibashi, and H. Kikuchi. Active matrix magneto-optical spatial light modulator driven by spin-transfer-switching. *Journal of Display Technology*, 12(10):1212–1217, 2016.
- [4] B. C. Kress and W. J. Cummings. Towards the ultimate mixed reality experience: Hololens display architecture choices. *SID Symposium Digest of Technical Papers*, 48, 2017.
- [5] O. Cakmakci, Y. Ha, and J. P. Rolland. A compact optical see-through head-worn display with occlusion support. In *3rd IEEE ISMAR*, pages 16–25, 2004.
- [6] K.-H. F. Chiang, S.-T. Wu, and S.-H. Chen. Fringing field effect of the liquid-crystal-on-silicon devices. *Japanese journal of applied physics*, 41(7R):4577, 2002.
- [7] T. Cui, B. Bai, and H.-B. Sun. Tunable metasurfaces based on active materials. *Advanced Functional Materials*, 29(10):1806692, 2019.
- [8] Z. Dong, J. Ho, Y. F. Yu, Y. H. Fu, R. Paniagua-Dominguez, S. Wang, A. I. Kuznetsov, and J. K. Yang. Printing beyond srgb color gamut by mimicking silicon nanostructures in free-space. *Nano letters*, 17(12):7620–7628, 2017.
- [9] L. Driencourt, F. Federspiel, D. Kazazis, L.-T. Tseng, R. Frantz, Y. Ekinci, R. Ferrini, and B. Gallinet. Electrically tunable multicolored filter using birefringent plasmonic resonators and liquid crystals. *ACS Photonics*, 7(2):444–453, 2019.
- [10] K.-H. Fan-Chiang, S.-T. Wu, and S.-H. Chen. Fringing-field effects on high-resolution liquid crystal microdisplays. *Journal of Display Technology*, 1(2):304, 2005.
- [11] J. L. Gabbard, J. E. Swan, J. Zedlitz, and W. W. Winchester. More than meets the eye: An engineering study to empirically examine the blending of real and virtual color spaces. In *2010 IEEE Virtual Reality Conference (VR)*, pages 79–86. IEEE, 2010.
- [12] C. Gao, Y. Lin, and H. Hua. Occlusion capable optical see-through head-mounted display using freeform optics. In *11th IEEE ISMAR*, pages 281–282, 2012.
- [13] C. Gao, Y. Lin, and H. Hua. Optical see-through head-mounted display with occlusion capability. In *Proc. SPIE*, volume 8735, pages 87350F–1:9, 2013.
- [14] T. Hamasaki and Y. Itoh. Varifocal occlusion for optical see-through head-mounted displays using a slide occlusion mask. *IEEE TVCG*, 25(5):1961–1969, 2019.
- [15] W. Harm, A. Jesacher, G. Thalhammer, S. Bernet, and M. Ritsch-Marte. How to use a phase-only spatial light modulator as a color display. *Optics letters*, 40(4):581–584, 2015.
- [16] Y. Itoh, T. Hamasaki, and M. Sugimoto. Occlusion leak compensation for optical see-through displays using a single-layer transmissive spatial light modulator. *IEEE TVCG*, 23(11):2463–2473, 2017.
- [17] Y. Itoh, T. Langlotz, D. Iwai, K. Kiyokawa, and T. Amano. Light attenuation display: Subtractive see-through near-eye display via spatial color filtering. *IEEE TVCG*, 25(5):1951–1960, May 2019.
- [18] Q. Jiang, G. Jin, and L. Cao. When metasurface meets hologram: principle and advances. *Advances in Optics and Photonics*, 11(3):518–576, 2019.
- [19] J. Kim, M. Stengel, J.-Y. Wu, B. Bouadaoud, J. Spjut, K. Akşit, R. Albert, T. Greer, Y. Jeong, W. Lopes, Z. Majercik, P. Shirley, M. McGuire, and D. Luebke. Matching prescription & visual acuity: Towards ar for humans. In *ACM SIGGRAPH 2019 Emerging Technologies*, SIGGRAPH 19. Association for Computing Machinery, New York, NY, USA, 2019.
- [20] K. Kim, D. Heo, and J. Hahn. Occlusion-capable head-mounted display. In *PHOTOOPTICS*, pages 299–302, 2019.
- [21] K. Kiyokawa, M. Billinghamurst, B. Campbell, and E. Woods. An occlusion-capable optical see-through head mount display for supporting co-located collaboration. In *2nd IEEE ISMAR*, page 133, 2003.
- [22] K. Kiyokawa, Y. Kurata, and H. Ohno. An optical see-through display for mutual occlusion of real and virtual environments. In *Augmented Reality, 2000.(ISAR 2000). Proceedings. IEEE and ACM International Symposium on*, pages 60–67. IEEE, 2000.
- [23] K. Kiyokawa, Y. Kurata, and H. Ohno. An optical see-through display for mutual occlusion with a real-time stereovision system. *CG*, 25(5):765–779, 2001.
- [24] G. A. Koulieris, K. Akit, M. Stengel, R. K. Mantiuk, K. Mania, and C. Richardt. Near-eye display and tracking technologies for virtual and augmented reality. *Computer Graphics Forum*, 38(2):493–519, 2019.
- [25] T. Kozacki and M. Chlipala. Color holographic display with white light led source and single phase only slm. *Optics Express*, 24(3):2189–2199, 2016.
- [26] B. Krajancich, N. Padmanaban, and G. Wetzstein. Factored occlusion: Single spatial light modulator occlusion-capable optical see-through augmented reality display. *IEEE TVCG*, 26(5):1871–1879, 2020.
- [27] T. Langlotz, M. Cook, and H. Regenbrecht. Real-time radiometric compensation for optical see-through head-mounted displays. *IEEE TVCG*, 22(11):2385–2394, Nov. 2016.
- [28] G. Lazarev, A. Hermerschmidt, S. Krüger, and S. Osten. Lcos spatial light modulators: trends and applications. *Optical Imaging and Metrology: Advanced Technologies*, pages 1–29, 2012.
- [29] G. Lazarev, A. Hermerschmidt, S. Krüger, and S. Osten. Lcos spatial light modulators: Trends and applications. *Optical Imaging and Metrology: Advanced Technologies*, pages 1–29, 2012.
- [30] C. Lingel, T. Haist, and W. Osten. Optimizing the diffraction efficiency of slm-based holography with respect to the fringing field effect. *Applied optics*, 52(28):6877–6883, 2013.
- [31] G. J. Lippmann. On colour photography by the interferential method. *Proceedings of the Royal society of London*, 60(359–367):10–13, 1897.
- [32] X. Luo. Subwavelength optical engineering with metasurface waves. *Advanced Optical Materials*, 6(7):1701201, 2018.
- [33] A. Maimone and H. Fuchs. Computational augmented reality eyeglasses. In *12th IEEE ISMAR*, pages 29–38, 2013.
- [34] D. J. Mitchell. Reflecting nature: chemistry and comprehensibility in gabriel lippmann's 'physical' method of photographing colours. *Notes and Records of the Royal Society*, 64(4):319–337, 2010.
- [35] N. Padmanaban, R. Konrad, and G. Wetzstein. Autofocals: Evaluating gaze-contingent eyeglasses for presbyopes. *Science advances*, 5(6):eaav6187, 2019.
- [36] M. Persson, D. Engström, and M. Goksör. Reducing the effect of pixel crosstalk in phase only spatial light modulators. *Optics express*, 20(20):22334–22343, 2012.
- [37] K. Rathinavel, G. Wetzstein, and H. Fuchs. Varifocal occlusion-capable optical see-through augmented reality display based on focus-tunable optics. *IEEE TVCG*, 25(11):3125–3134, 2019.
- [38] M. Shih, A. Shishido, and I. Khoo. All-optical image processing by means of a photosensitive nonlinear liquid-crystal film: edge enhancement and image addition–subtraction. *Optics letters*, 26(15):1140–1142, 2001.
- [39] M. Song, X. Li, M. Pu, Y. Guo, K. Liu, H. Yu, X. Ma, and X. Luo. Color display and encryption with a plasmonic polarizing metamirror. *Nanophotonics*, 7(1):323–331, 2018.
- [40] S. K. Sridharan, J. D. Hincapie-Ramos, D. R. Flatla, and P. Irani. Color correction for optical see-through displays using display color profiles. In *Proceedings of the 19th ACM Symposium on Virtual Reality Software and Technology*, pages 231–240, 2013.
- [41] I. E. Sutherland. A head-mounted three dimensional display. In *Proceedings of the December 9–11, 1968, fall joint computer conference, part I*, pages 757–764, 1968.
- [42] S. J. Tan, L. Zhang, D. Zhu, X. M. Goh, Y. M. Wang, K. Kumar, C.-W. Qiu, and J. K. Yang. Plasmonic color palettes for photorealistic printing with aluminum nanostructures. *Nano letters*, 14(7):4023–4029, 2014.
- [43] E. W. Tatham. Technical opinion: Getting the best of both real and virtual worlds. *ACM Communications*, 42(9):96–98, 1999.
- [44] K. Thyagarajan, R. Sokhoyan, L. Zornberg, and H. A. Atwater. Millivolt modulation of plasmonic metasurface optical response via ionic conductance. *Advanced Materials*, 29(31):1701044, 2017.
- [45] M. L. Tseng, J. Yang, M. Semmlinger, C. Zhang, P. Nordlander, and N. J. Halas. Two-dimensional active tuning of an aluminum plasmonic array for full-spectrum response. *Nano letters*, 17(10):6034–6039, 2017.
- [46] T. Uchida, K. Sato, and S. Inokuchi. An optical see-through mr display with digital micro-mirror device. *Trans. of the Virtual Reality Society of Japan*, 7(2), 2002.
- [47] G. Wetzstein, W. Heidrich, and D. Luebke. Optical image processing using light modulation displays. *Computer Graphics Forum*, 29(6):1934–1944, 2010.
- [48] A. Wilson and H. Hua. Design and prototype of an augmented reality display with per-pixel mutual occlusion capability. *Opt. Express*, 25(24):30539–30549, 2017.

- [49] S.-T. Wu and U. Efron. Optical properties of thin nematic liquid crystal cells. *Applied physics letters*, 48(10):624–626, 1986.
- [50] S.-T. Wu, U. Efron, and L. D. Hess. Birefringence measurements of liquid crystals. *Applied optics*, 23(21):3911–3915, 1984.
- [51] T. Xu, Y.-K. Wu, X. Luo, and L. J. Guo. Plasmonic nanoresonators for high-resolution colour filtering and spectral imaging. *Nature communications*, 1(1):1–5, 2010.
- [52] Y. Yamaguchi and Y. Takaki. See-through integral imaging display with background occlusion capability. *Applied Optics*, 55(3):A144–A149, 2016.